HOKKAIDO UNIVERSITY

Title	Corrosion protection of iron using porous anodic oxide/conducting polymer composite coatings
Author(s)	Konno, Yoshiki; Tsuji, Etsushi; Aoki, Yoshitaka et al.
Citation	Faraday discussions, 180, 479-493 https://doi.org/10.1039/c4fd00232f
Issue Date	2015
Doc URL	https://hdl.handle.net/2115/62391
Type	journal article
File Information	Habazaki-FD.pdf

Hokkaido University Collection of Scholarly and Academic Papers : HUSCAP

CREATED USING THE RSC REPORT TEMPLATE (VER. 3.1) - SEE WWW.RSC.ORG/ELECTRONICFILES FOR DETAILS

Corrosion Protection of Iron Using Porous Anodic Oxide/Conducting Polymer Composite Coatings

Yoshiki Konno,[a] Etsushi Tsuji,[a,b] Yoshitaka Aoki,[a,b] Toshiaki Ohtsuka[b] and Hiroki Habazaki[a,b,*]

DOI: 10.1039/b000000x [DO NOT ALTER/DELETE THIS TEXT]

Conducting polymers (CPs), including polypyrrole, have attracted attention for their potential in the protection of metals against corrosion; however, CP coatings have the limitation of poor adhesion to metal substrates. In this study, a composite coating comprising a self-organized porous anodic oxide layer and a polypyrrole layer has been developed on iron. Because of electropolymerization in the pores of the anodic oxide layer, the composite coating showed improved adhesion to the substrate along with prolonged corrosion protection in NaCl aqueous corrosive environment. The anodic oxide layers are formed in fluoride-containing organic electrolyte and contain a large amount of fluoride species. The removal of these fluoride species from the oxide layer and the metal/oxide interface region is crucial for improving the corrosion protection.

1 Introduction

The use of conducting polymers (CPs) for the corrosion protection of metals has attracted considerable attention over the past decades. Oxidative properties of CPs maintain the potential of the substrate in the passive state.[1, 2] Polypyrrole (PPy), one of the CPs, is often studied for corrosion protection of metals and can be readily deposited on steel by electropolymerization in aqueous electrolytes. During the electropolymerization of pyrrole, electrolyte anions are incorporated into the PPy film, and the nature of the incorporated anions significantly influences the properties of the resultant PPy films.[3-5] The incorporated anions are released during the reduction of PPy. Inhibitor anions are preferable as incorporated species because they protect metals from corrosion. In fact, PPy films with incorporated molybdate[6-10] and molybdophosphate[11-13] have shown good corrosion protection of metals. Release of such inhibitor anions into corrosive solutions can be suppressed by the introduction of an outer PPy layer with incorporated large organic anions, which inhibit the decomposition and release of molybdophosphate ions in the inner layer.[12] Such bi-layer coating further improves the corrosion protection properties.

[a] *Graduate School of Chemical Sciences and Engineering, Hokkaido University, Sapporo, Hokkaido 060-8628, Japan*
[b] *Faculty of Engineering, Hokkaido University, Sapporo, Hokkaido 060-8628, Japan. Tel & Fax: +81-11-706-6575; E-mail: habazaki@eng.hokudai.ac.jp*

This journal is © The Royal Society of Chemistry [year]

Although the CPs are promising for corrosion protection and extensive studies have been conducted regarding their corrosion protection properties, one of the important issues which must be addressed to fulfil the requirements of high-performance corrosion-protection coatings under widely varying practical conditions is the poor adhesion of the coatings to the metal substrate. In the present study, self-organized porous anodic films are introduced between the iron substrate and the PPy layer to further improve the adhesion and corrosion protection properties.

Anodizing of aluminium in acid electrolytes develops self-organized porous anodic films, which have been widely used in industry for corrosion protection, wear resistance and colouring of aluminium and its alloys. The formation of such self-organized nanoporous and nanotubular anodic films has been recently extended to other metals such as titanium, zirconium, niobium, tantalum and tungsten.[14]

Anodizing of iron in aqueous electrolytes at high potentials results in the formation of soluble ferrate ions[15, 16] such that no porous anodic films can be formed on iron. However, recent reports disclosed that nanoporous and nanotubular anodic films were formed on iron in ethylene glycol or glycerol electrolyte containing fluoride and small amounts of H_2O.[17-22] The anodic films thus formed are mainly amorphous and highly contaminated with fluoride species; however, they are readily converted to nanoporous or nanotubular α-Fe_2O_3, which is of potential interest as a photoanode for water splitting,[17, 20, 23] as a photoelectrocatalyst[24] and as electrodes in electrochemical capacitors.[25] In the pores of the anodic oxide on iron, it is expected that PPy is deposited by the electropolymerization of pyrrole, similar to electropolymerization in porous anodic alumina templates.[26] In this case, the PPy layer prepared on the anodized iron substrate should exhibit improved adhesion due to anchor effect.

In the present study, PPy/anodic oxide composite coatings have been prepared. The anodic films on iron have been prepared by anodizing iron in ethylene glycol electrolyte containing NH_4F and H_2O. The resultant films contain large amounts of fluoride and dissolve readily in aqueous solutions. Thus, thermal treatment is required to remove fluoride species and to form crystalline iron oxide phases. The conditions of thermal treatment for the removal of fluoride species have also been examined. Electropolymerization to produce a PPy layer has been performed in phosphoric acid aqueous electrolyte containing pyrrole monomer and molybdophosphate, which acts as an inhibitor as well as a dopant.

2 Experimental

2.1 Formation of anodic films

High purity (99.99%) iron plate was used as a substrate, which was mechanically polished with 1500 grit SiC polishing paper. After degreasing in acetone ultrasonically, the iron specimens were anodized at a constant voltage of 35 V in ethylene glycol electrolyte containing 0.1 mol L^{-1} NH_4F and 0.5 mol L^{-1} H_2O at 313 K for 300 s. After anodizing, the resultant anodic film was dissolved under cathodic polarization conditions of 200 A m^{-2} in 0.1 mol L^{-1} HCl solution. Then, the iron specimen was re-anodized under the same conditions. This two-step anodizing was performed to obtain a smoother substrate surface than that obtained after the first anodizing step. After anodizing, the specimen was ultrasonically washed in ethylene glycol followed by acetone.

The thermal treatment of the anodized specimens was conducted either in air or

This journal is © The Royal Society of Chemistry [year]

argon at temperatures between 523 K and 673 K for 1.8 ks. Heating rate at the selected temperature was 2.5 K min^{-1}. A relatively slow heating rate was selected to avoid cracking of the anodic oxide layer. After the thermal treatment, the specimen was gradually cooled to room temperature in the furnace.

2.2 Formation of the PPy layer

The PPy layer was formed on the anodized specimens and subsequently on thermally-treated iron and passivated iron specimens. The passivation treatment of iron was performed at 0.8 V vs. Ag/AgCl in 0.06 mol L^{-1} Na_2MoO_4 aqueous solution for 15 min. For the electropolymerization of PPy, a three-electrode cell with an Ag/AgCl reference electrode and a platinum foil counter electrode was used. The electrolyte was 0.2 mol L^{-1} H_3PO_4 solution containing 0.1 mol L^{-1} pyrrole monomer and 5 mmol L^{-1} $H_3PMo_{12}O_{40}$. The solution was prepared in deionized milli-Q water and then deoxygenated by nitrogen bubbling for 30 min prior to use. The electropolymerization was performed at a constant current density of 10 A m^{-2} for 30 min at room temperature to deposit an approximately 5-μm-thick PPy layer.

2.3 Characterization of coatings

Surfaces and cross-sections of the coated specimens were observed by a JEOL JSM-6500F field emission-scanning electron microscope (FE-SEM) operated at 10 kV. Some cross-sections of the anodized and thermally treated iron specimens were also observed by a JEOL JEM-2010 transmission electron microscope (TEM) operated at 200 kV and a Hitachi HD-2000 scanning transmission electron microscope (SEM) operated at 200 kV. Electron-transparent sections were prepared by a Hitachi FB-2100 FIB system employing a Ga^+ ion beam. Phases in the porous anodic layers were identified using a Rigaku RINT2000 X-ray diffractometer (XRD) using Cu Kα irradiation. Both θ-2θ and α-2θ modes with α = 1° were used to obtain information regarding the depth distribution of individual phases.

Elemental depth profile analysis was performed using a Jobin-Yvon 5000 RF glow discharge optical emission spectroscopy (GDOES) instrument in a neon atmosphere of 1100 Pa by applying an RF of 13.56 MHz and a power of 50 W. Neon gas was used to excite emissions from fluorine because no excitation is observed with the conventional argon gas.[27] Light emissions of characteristic wavelengths were monitored throughout the analysis with a sampling time of 0.1 s to obtain depth profiles. The wavelengths of spectral lines used were 121.567 nm for hydrogen, 165.701 nm for carbon, 130.217 nm for oxygen, 685.602 nm for fluorine, 178.287 nm for phosphorus, 385.991 nm for iron and 317.035 nm for molybdenum. Signals were detected from a circular area of approximately 4 mm diameter.

Adhesion of the coatings to the iron substrate was evaluated by a cross-cut test (ISO-2409). The corrosion tests of the coated specimens were performed by immersing in 3.5 wt% NaCl solution at room temperature and continuously recording the corrosion potential.

3 Results and Discussion

3.1 Formation of a nanoporous anodic film

Nanoporous anodic films on iron can be prepared in ethylene glycol electrolytes

This journal is © The Royal Society of Chemistry [year]

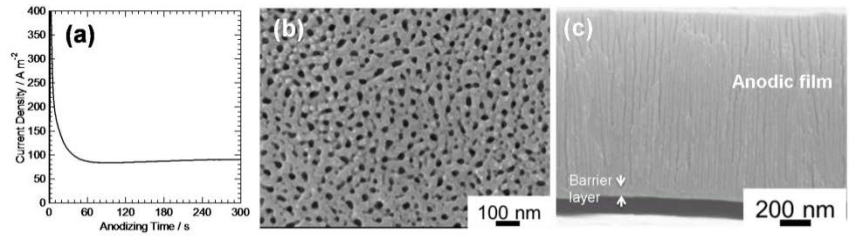

Fig. 1 (a) Current transient of iron during anodizing at 35 V in ethylene glycol electrolyte containing 0.1 mol L^{-1} NH_4F and 0.5 mol L^{-1} H_2O at 313 K for 300 s; scanning electron micrographs of (b) surface and (c) fracture cross-section of the resultant anodic film.

containing NH_4F and H_2O.[21, 28] In this study, we developed the anodic film by anodizing at 35 V in ethylene glycol electrolyte containing 0.1 mol L^{-1} NH_4F and 0.5 mol L^{-1} H_2O at 313 K for 300 s. The current transient during anodizing (Fig. 1a) reveals an initial current decay to a steady-state current density of approximately 90 A m^{-2} within 60 s. SEM image of the surface of the anodized specimen (Fig. 1b) discloses the formation of a nanoporous anodic film with a pore size of ~30 nm. Cross-sectional observation (Fig. 1c) reveals the development of cylindrical nanopores in the anodic film. These nanopores are grown in the direction normal to the metal/film interface, as in the case of the well-known porous anodic alumina films formed in acidic aqueous electrolytes such as sulphuric acid, oxalic acid and phosphoric acid.[29] The thickness of the anodic film is 1.2 μm, and a thin barrier layer (~60 nm) is also observed at the bottom of the anodic film, corresponding to the ratio of the thickness of the barrier layer to the formation voltage of 1.7 nm V^{-1}. This value is slightly smaller than that observed at 293 K (1.9 nm V^{-1}).[21] The ratio usually increases with an increase in electrolyte temperature because of the reduction of field strength at higher temperatures. This reduction may be associated with a change in film composition, such as the amounts of incorporated electrolyte species in the anodic film, although more detailed study is required for clarification. In the fractured cross-section (Fig. 1c), the anodic film is separated from the iron substrate, which probably occurs during the preparation of the cross-section. The anodic film is highly contaminated with fluoride species, as discussed later, and fluoride-rich anodic films often have poor adhesion to metal substrates.[30,31] The formation of a fluoride-containing anodic film could be one of the reasons for the detachment of the anodic film from the substrate.

3.2 Thermal treatments to remove fluoride species

The anodic film formed on iron in the present electrolyte contains a large amount of fluoride species, and the film is soluble even in water. To remove the fluoride species and form more chemically stable oxide films, thermal treatments of the anodized specimens were performed. SEM images of the specimens that were thermally treated up to 673 K, both in air and argon, revealed a nanoporous surface morphology similar to Fig. 1b. No obvious change in surface pore morphology occurred during thermal treatments.

Fig. 2 shows the SEM images of the cross-sections of the anodized specimens after thermal treatments at different temperatures in air and argon. Vertically aligned

This journal is © The Royal Society of Chemistry [year]

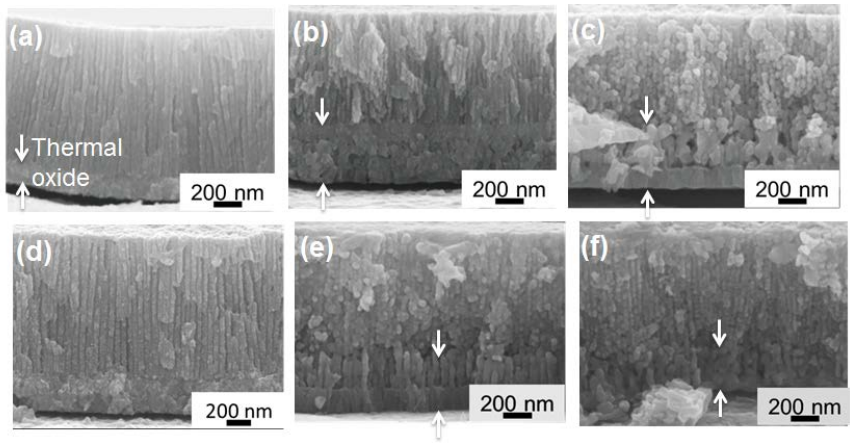

Fig. 2 Scanning electron micrographs of cross-sections of the anodized iron specimens after thermal treatment in air at (a) 523 K, (b) 623 K and (c) 673 K and in argon at (d) 523 K, (e) 623 K and (f) 673 K.

nanopores are still present even after thermal treatment, although nanogranular materials are developed at higher temperatures. At the bottom of the anodic film, the growth of thermal oxide appears to proceed during thermal treatment. When thermal treatment is performed at 673 K, the thermal oxide layer consists of two layers, an inner compact layer and an outer porous layer. The pore walls in the outer thermal oxide layer are significantly thicker than those in the anodic porous layer, which is located above the thermal oxide layer.

The change in the film thickness with the temperature of thermal treatment depends upon the atmosphere (Fig. 3). The total thickness of the oxide layer is almost constant even after thermal treatment in air at several temperatures, although thermal oxide layers tend to thicken with the temperature of thermal treatment. This is possibly due to the outward diffusion of iron species in the thermal oxide layer during thermal treatment; the outward diffusing iron species form a new oxide material at the pore base, implying that the oxide formation at the oxide/substrate interface is negligible. In contrast, the total film thickness increases from 1.2 μm to 1.5 μm after thermal treatment in argon at 523 K without significant change in the

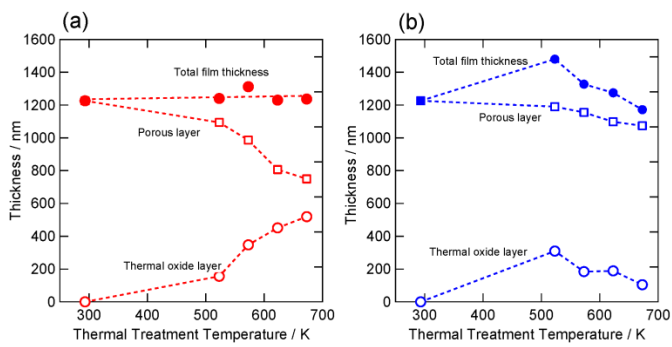

Fig. 3 Change in the thickness of the oxide layers on the anodized iron specimens with the temperature of thermal treatment in (a) air and (b) argon atmospheres.

This journal is © The Royal Society of Chemistry [year]

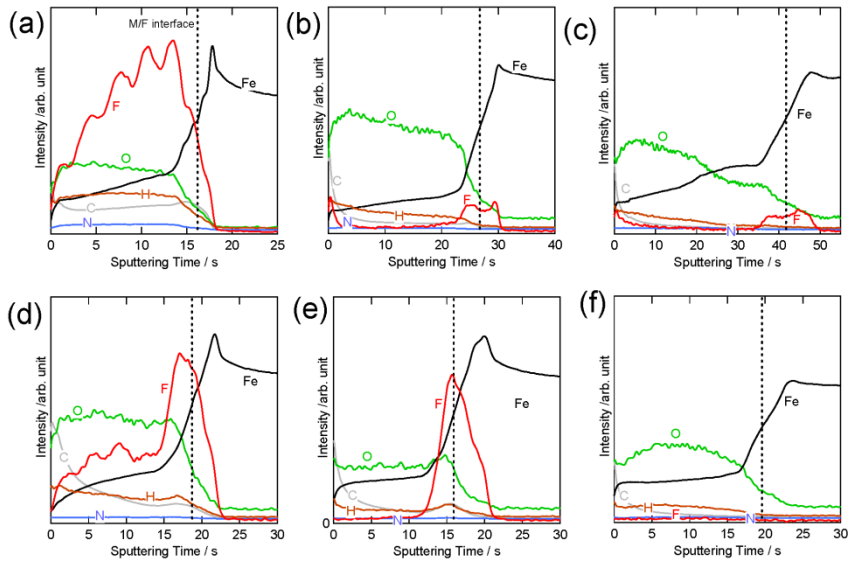

Fig. 4 GDOES depth profiles of the anodized specimens (a) before and after thermal treatment in air at (b) 523 K and (c) 673 K and in argon at (d) 523 K, (e) 623 K and (f) 673 K.

thickness of the porous layer. A thermal oxide layer (~300 nm thick) appears to be formed without filling pores, i.e. at the oxide/metal interface due to the inward diffusion of anions. A trace amount of impurity oxygen in the argon atmosphere may contribute to the formation of thermal oxide.

The total film thickness decreases gradually from 1.5 μm to ~1.2 μm with an increase in the temperature of thermal treatment, mainly due to the thinning of the thermal oxide layer. The reduction of the thickness of the porous layer is limited compared with the thermal treatment in air.

The removal of the fluoride species from the anodic film by thermal treatment was examined by GDOES depth profile analysis. It is clear from Fig. 4a that the as-anodized specimen contains a relatively large amount of fluoride species throughout the anodic film. The film also contains carbon and nitrogen species which are probably derived from ethylene glycol and ammonium ions, respectively. Incorporation of such species increases the solubility of the anodic film in water.

After thermal treatment in air at 523 K (Fig. 4b), the fluoride species in the anodic film becomes negligible and the intensities of carbon and nitrogen are remarkably reduced; the anodic film is converted to an oxide-based layer. However, the fluoride species are still present at a depth close to the metal/oxide interface. The fluoride species located near the metal/oxide interface could not be fully removed even after thermal treatment at 673 K in air (Fig. 4c).

As discussed above, iron species diffuse outward in the thermal oxide layer during its growth in air. A new iron oxide is developed at the pore base. The formation of such oxides above the fluoride-containing layer may impede the removal of fluoride during thermal treatment.

Thus, we also carried out thermal treatment in an inert atmosphere. When thermal treatment is performed in argon at 523 K, a considerable amount of the fluoride species still remain in the anodic film (Fig. 4d). Because the amount of the fluoride

This journal is © The Royal Society of Chemistry [year]

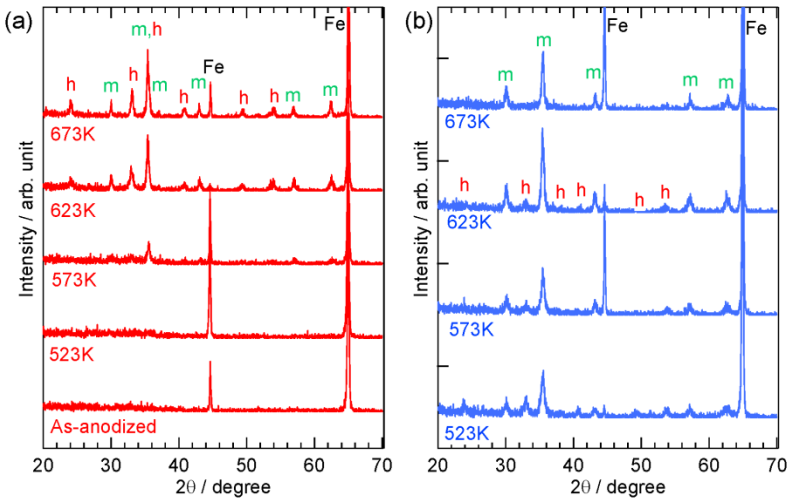

Fig. 5 XRD patterns of the anodized iron specimens before and after thermal treatment in (a) air and (b) argon at several temperatures; m: Fe_3O_4, h: α-Fe_2O_3.

species is negligible in the anodic film, except near the metal/oxide interface, after thermal treatment in air at the same temperature (Fig. 4b), it can be concluded that fluoride removal from the anodic film is accelerated in an air atmosphere compared with that in an argon atmosphere. The removal of the carbon species is also not sufficient at 523 K in argon. The fluoride species are removed from the anodic film after thermal treatment in argon at 623 K, but not from the region near the metal/oxide interface. However, after thermal treatment in argon at 673 K, the presence of the fluoride species near the interface becomes negligible, even though thermal treatment in air cannot remove the fluoride species near the interface. The suppression of outward diffusion of iron species to form an oxide layer above the fluoride-containing layer may be a necessary condition for the removal of fluoride from the metal/oxide interface region.

Phase transformation of the anodic film by thermal treatment was examined by XRD measurements. Fig. 5 shows the θ-2θ mode XRD patterns of the anodized iron specimens before and after thermal treatment under various conditions. The as-anodized specimen reveals reflections only from the iron substrate, indicating that the anodic film is amorphous or poorly crystalline. Reflections of crystalline oxides appear when thermal treatment in air is performed at 573 K. The reflections become more intense with an increase in temperature. Reflections of both Fe_3O_4 and α-Fe_2O_3 are observed after thermal treatment at or above 623 K. From a comparison with the respective α-2θ mode XRD pattern, in which the relative intensity of α-Fe_2O_3 reflections is enhanced, the porous layer formed by anodizing appears to be converted mainly to α-Fe_2O_3, whereas Fe_3O_4 is mainly formed by the thermal oxidation of the iron substrate.

When thermal treatment was performed in an argon atmosphere, both Fe_3O_4 and α-Fe_2O_3 are formed even at 523 K, although fluoride species are remained as shown in Fig. 4d. Since no oxide phases are observed at this temperature in air (Fig. 4a), it can be said that an amorphous-to-crystalline transition is accelerated in an argon atmosphere at a low oxygen partial pressure, compared with in air. At a higher

This journal is © The Royal Society of Chemistry [year]

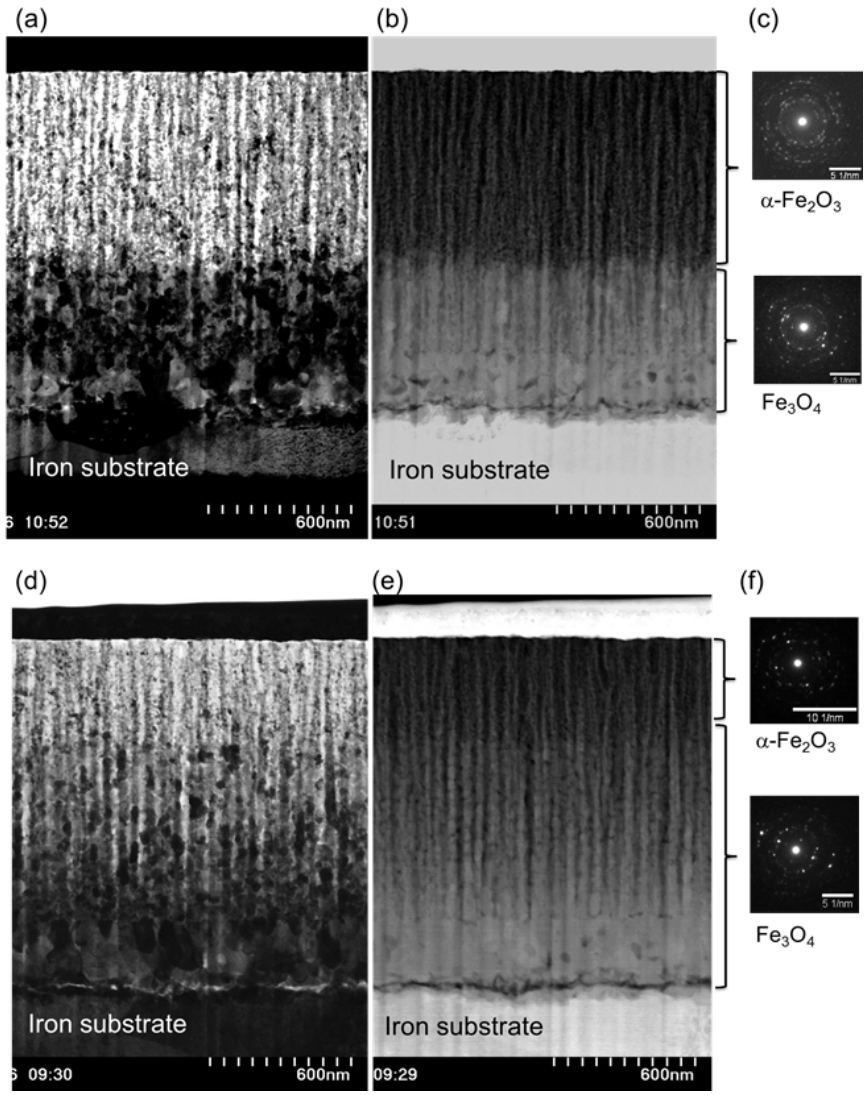

Fig. 6 Scanning transmission electron micrographs of FIB cross-sections of the anodized iron specimens after thermal treatment in (a-c) air and (d-f) argon at 673 K; (a,d) bright field images, (b,e) HAADF images and (c,f) selected area electron diffraction patterns.

temperature of 673 K, at which fluoride species are removed, only Fe_3O_4 reflections are observed. However, in the α-2θ mode XRD pattern (α = 1°), weak α-Fe_2O_3 reflections were also detected, suggesting that the outer α-Fe_2O_3 layer may become thinner in argon.

The anodized iron specimens thermally treated at 673 K in air and argon were further examined by TEM. Fig. 6a shows the bright field transmission electron micrograph of an FIB cross-section of the anodized specimen after thermal treatment

This journal is © The Royal Society of Chemistry [year]

in air at 673 K. Obviously, vertically aligned nanopores are developed in agreement with the SEM observations (Fig. 2c). Apparently, the oxide layer is divided into two regions from contrast. From the HAADF image (Fig. 6b), it is clear that each oxide layer has different composition. A selected area electron diffraction (SAED) pattern of the outer layer with a dark appearance in the HAADF image discloses the presence of α-Fe_2O_3 in this layer. The remaining inner dark layer in Fig. 6a, corresponding to the thermal oxide layer shown in Fig. 2c, mainly consists of Fe_3O_4 from the SAED pattern. Because of its higher oxygen content, the outer layer shows a relatively dark appearance in the HAADF image. It can be confirmed that the anodic porous layer is converted to α-Fe_2O_3, and the Fe_3O_4 phase is mainly formed in association with the thermal oxidation of the iron substrate.

In contrast, the thermal treatment in argon results only in the formation of α-Fe_2O_3 in the outer ~300 nm thickness of the porous layer, as shown in Figs. 6d–f. The main part of the oxide layer consists of Fe_3O_4, which is in agreement with the XRD patterns. The grain size of α-Fe_2O_3 is relatively small, i.e. less than 50 nm. This size is limited by the thickness of pore walls. Larger grains of Fe_3O_4 are developed in agreement with Fig. 2. The grain size of each phase is almost independent of the atmosphere of thermal treatment.

3.3 Electropolymerization of PPy

A PPy layer was formed on the anodized iron specimens after thermal treatment. Fig. 7a shows the potential transient during electropolymerization at a constant current density of 10 A m^{-2}. The electropolymerization proceeded at a steady-state potential of 0.6 V vs. Ag/AgCl on the passivated iron substrate without an anodic film. The iron specimen anodized and thermally treated in argon at 673 K shows similar electropolymerization potential. In contrast, the steady-state potential increases to higher than 1.4 V for iron specimens that were anodized and thermally treated in air. The potential increases gradually with the temperature of thermal treatment. Such high electropolymerization potentials may be associated with the high electric

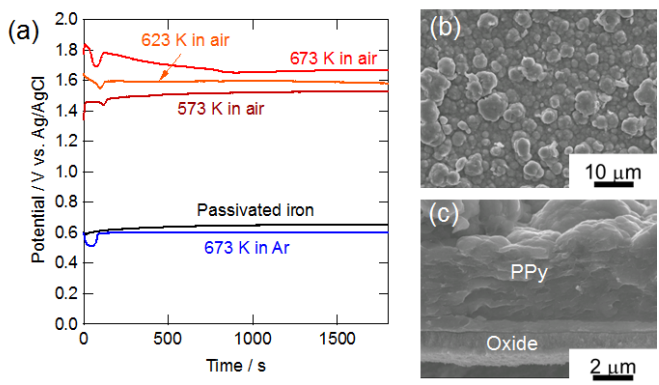

Fig 7. (a) Potential transients during electrosynthesis of PPy on iron specimens with and without porous oxide layers thermally treated at several temperatures in air and argon; scanning electron micrographs of (b) surface and (c) cross-section of the PPy/porous oxide-coated specimen with thermal treatment in argon at 673 K.

This journal is © The Royal Society of Chemistry [year]

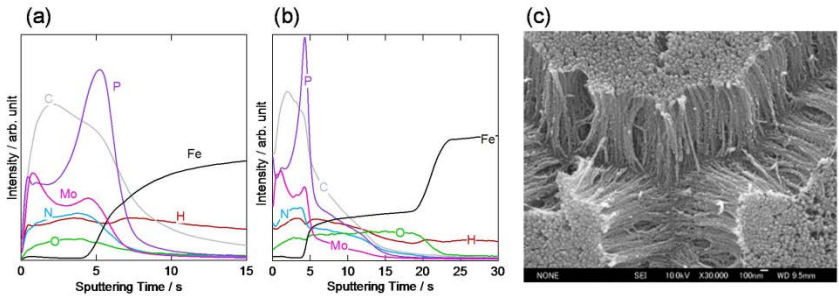

Fig. 8 GDOES depth profiles of the iron specimens with (a) PPy coating and (b) PPy/anodic oxide composite coating with thermal treatment in argon at 673 K and (c) scanning electron micrograph of PPy nanofibers formed in the porous anodic layer thermally treated in argon at 673 K. The nanofibers were observed after chemical dissolution of iron and the anodic oxide layer in HCl solution.

resistivity of the oxide layer formed in air at elevated temperatures. When the iron specimens anodized and thermally treated in argon at or below 623 K were used, electropolymerization to form a PPy layer was unsuccessful. In the electropolymerization electrolyte, the oxide layer was detached because of the presence of relatively high amounts of fluoride species near the metal/oxide interface.

The deposition of PPy was confirmed by SEM observations (Figs. 7b,c). The PPy layer is deposited relatively homogenously with a globular morphology (Fig. 7b), which is typical of electrosynthesized PPy.[12] The thickness of the PPy layer is approximately 5 μm (Fig. 7c).

The deposition of PPy in the nanopores of the iron oxide layer was evident from the GDOES depth profiles (Fig. 8). The deposited PPy contains incorporated anion species. Thus, the penetration of PPy into the nanopores of the oxide layer can be evaluated from the presence of molybdenum and phosphorus species in the oxide layer. This is evident from the depth profile of the PPy layer formed on the passivated iron (Fig. 8a). The PPy layer contains carbon, nitrogen, hydrogen, molybdenum, phosphorus and oxygen with the latter three derived from the incorporated anion species. The depth profile of phosphorus is different from molybdenum, suggesting that phosphate derived from phosphoric acid may also be incorporated in addition to molybdophosphate anions. For the anodized specimens with thermal treatments in argon at 673 K (Fig. 8b), it is obvious that PPy penetrates into the pores of the oxide layer from molybdenum, carbon and phosphorus profiles. The absence of these species in the inner oxide layer is because of the formation of the thermal oxide layer. A comparison of the relative intensities of nitrogen, molybdenum and phosphorus in Fig. 8b is interesting. With respect to the intensity of nitrogen, derived from PPy, the intensity of molybdenum, derived from incorporated anions, becomes lower in the porous anodic oxide layer compared with the outer PPy layer; the intensity of molybdenum in the outer PPy layer is higher than that of nitrogen, whereas the intensity of the former becomes approximately half of the latter in the porous anodic oxide layer. Similar result is obtained for phosphorus intensity with respect to the intensity of nitrogen. The depth profile of the outer PPy layer in Fig. 8b is similar to that of the PPy layer in Fig. 8a, which suggests that anion incorporation is reduced in the nanopores of the anodic oxide

This journal is © The Royal Society of Chemistry [year]

layer.

The electropolymerization of pyrrole proceeds via the reactions shown in Scheme 1. The pyrrole monomer is oxidized on the anode to form a neutral polymer. This polymer is further oxidized to produce positive charges which are compensated by doped anions. Because the neutral polymer does not have a high conductivity, the doping process is indispensable for increasing the conductivity of the polymer. Lower concentration of doping anions in the nanopores of the porous anodic oxide layer, in comparison with the outer PPy layer, suggests that either the available anions are limited in the nanopores electrolyte or only limited doping occurs during electropolymerization in the nanopores.

Different concentrations of anions in the nanopores and bulk solution were recently demonstrated in porous silicon.[32] Depending upon the concentration and size of the anions, the deposition of platinum in the nanopores of silicon was markedly influenced. Therefore, it is possible that the concentration of anions in the nanopores of the porous anodic layer in the present study is also different from that in the bulk solution. For a more detailed understanding, the influence of the type of anions, pore size and pore wall hydrophobicity is under investigation.

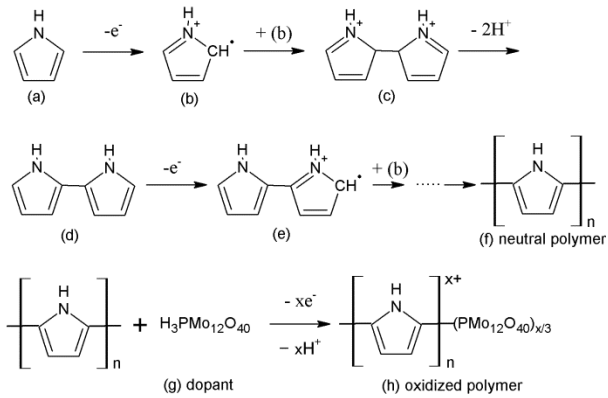

Scheme 1 Reactions during anodic oxidation of the pyrrole monomer in the presence of $H_3PMo_{12}O_{44}$.

Fig. 8c shows the SEM image of PPy nanofibers deposited in the oxide nanopores. Nanofibers were observed after chemical dissolution of the oxide layer and iron substrate in HCl solution. The presence of PPy nanofibers indicates the deposition of PPy into the nanopores of the oxide layer. The length of the nanofibers is approximately 1.2 μm, corresponding to the thickness of the porous oxide layer. Similar penetration of PPy into the porous anodic oxide layer was also confirmed for the specimens thermally treated in air.

3.4 Adhesion and corrosion resistance

The adhesion of the coatings to the iron substrate was examined by a cross-cut test. The PPy layer deposited on the passivated iron revealed detachment in more than 60% of the area, indicating insufficient adhesion of the PPy layer to the substrate. For the PPy/anodic oxide composite coatings thermally treated in air, adhesion is improved but detachment always occurred at the substrate/oxide layer interface

This journal is © The Royal Society of Chemistry [year]

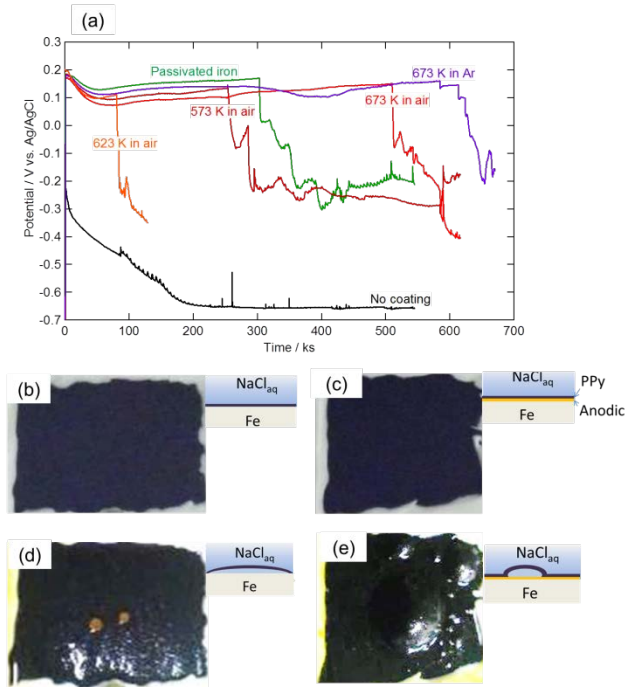

Fig. 9 (a) Change in the open circuit potential of the non-coated and coated iron specimens during immersion in 3.5 wt% NaCl solution; PPy coating was performed on anodized iron substrates with thermal treatment in air and argon at several temperatures and passivated iron substrate. Specimen photos and schematic illustrations (b,d) before and (c,e) after immersion of (b,c) the PPy-coated specimen and (d,e) PPy/anodic oxide composite coated specimen with thermal treatment in argon at 673 K.

mainly due to the presence of the fluoride species near the interface. In contrast, detachment at the substrate/oxide layer interface never occurred for the coatings thermally treated at 673 K. As discussed above, the presence of fluoride in this specimen is negligible, suggesting that the removal of the fluoride species is of crucial importance for improving the adhesion of coatings.

The corrosion tests of the PPy and PPy/anodic oxide coated iron specimens were examined in 3.5% NaCl solution. Open circuit potential (OCP) was measured during the immersion of the coated and non-coated specimens (Fig. 9). The non-coated iron specimen shows an initial potential of −0.22 V vs. Ag/AgCl, which is within the active dissolution region. This potential further decreases to a steady-state potential of −0.65 V vs. Ag/AgCl. In contrast, the PPy-coated specimen exhibits a considerably higher potential of 0.2 V vs. Ag/AgCl at the commencement of immersion, which is in the passive region. This relatively high potential is because of the oxidative properties of the PPy layer. The high OCP of >0.1 V vs. Ag/AgCl is maintained for a certain period of time, during which no obvious corrosion occurs. Corrosion occurs after an abrupt decrease in the OCP to −0.2 V vs. Ag/AgCl. Thus, the durability of the PPy coatings can be evaluated from the duration for which a high OCP is maintained.

The PPy-coated, passivated iron specimen maintains the passive and protective state for ~300 ks. The protective duration is shorter for the PPy/anodic oxide

This journal is © The Royal Society of Chemistry [year]

composite coatings when the thermal treatment is performed in air at or below 623 K. The highest durability is obtained for the composite coating thermally treated in argon at 673 K, with negligible fluoride species. Because all the composite coatings with thermal treatment in air contain the fluoride species near the metal/oxide interface, their removal may be one of the important factors influencing the durability of the coating. In the presence of the fluoride species, the adhesion of the coatings is not directly correlated with the durability of corrosion protection because the composite coating with thermal treatment in air at 623 K, showing the shortest durability, exhibited better adhesion in comparison with the PPy coating without an anodic layer.

The composite coating with thermal treatment in argon at 673 K exhibits twice as long durability compared with the PPy coating without an anodic oxide layer. The improved adhesion of the coating on the substrate may impede the penetration of the

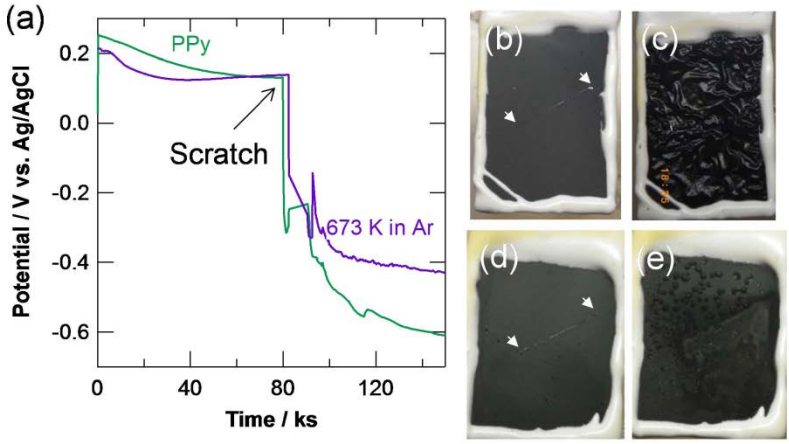

Fig. 10 (a) Change in the open circuit potential of the PPy-coated specimens with and without the anodic oxide layer thermally treated in argon at 673 K during immersion in 3.5 wt% NaCl solution. The specimens were scratched during immersion. Photos (b, d) just after scratching and (c, e) after 1 h from the scratching for the PPy-coated specimens (d, e) with and (b, c) without the anodic oxide layer.

corrosive solution into the coating/metal substrate interface. In addition, the presence of the thermal oxide barrier layer and the porous oxide layer together with the PPy layer may also improve the barrier nature of the coating. As shown in Figs. 9b-c, the PPy-coated specimen without an anodic oxide layer blisters over the entire surface, whereas blisters form in a limited area for the composite coating thermally treated in argon at 673 K. The presence of the adherent anodic oxide layer appears to suppress the expansion of corrosion over the entire surface.

During immersion in the NaCl solution, the PPy-coated specimen and PPy/anodic oxide composite-coated specimen with thermal treatment in argon at 673 K were scratched (Fig. 10). After scratching, the OCP decreases steeply and corrosion commenced at the scratched region for both the specimens. However, significant difference appears on the coatings within 1 h after scratching. For the PPy-coated specimen without anodic oxide, the coating is detached from the substrate on the entire surface exposed to the corrosive solution (Fig. 10b). Thus, the corrosion

This journal is © The Royal Society of Chemistry [year]

expanded on the entire surface within 1 h after scratching. Because of insufficient adhesion of PPy, the corrosive solution may penetrate into the coating/metal interface, accelerating the detachment and corrosion. In contrast, the composite coating is still adherent to the substrate even after scratching and the corrosion is apparently limited to the scratched region (Fig. 10c). The extension of corrosion on the entire surface is effectively suppressed by the composite coating with better adhesion to the substrate.

4 Conclusions

In summary, the present study demonstrates the beneficial role of the porous anodic oxide layer in corrosion protection of iron by PPy coating. The PPy/anodic oxide composite coating on iron remarkably improves the durability of the protective coating in NaCl solution compared with the PPy single coating. This improved adhesion to the substrate may be one of the reasons for the improved durability. The nanoporous anodic films were formed in ethylene glycol electrolyte containing NH_4F and H_2O. The resultant anodic film is amorphous and contains a relatively high concentration of fluoride, such that the as-formed film is chemically unstable. Thermal treatment converts the amorphous material to a mixture of α-Fe_2O_3 and Fe_3O_4 with the former forming the outer layer. However, thermal treatment in air cannot remove the fluoride near the metal/oxide interface. The formation of thermal oxide by outward diffusion of iron species inhibits the removal of the fluoride present beneath the developed oxide layer. Almost complete removal of fluoride is achieved by thermal treatment in argon at 673 K. The composite coating with this thermal treatment exhibits the longest durability for corrosion protection.

Acknowledgments

A part of this work was supported by the “Nanotechnology Platform” Program of the Ministry of Education, Culture, Sports, Science and Technology (MEXT), Japan.

References

1. B. Wessling, *Adv. Mater.*, 1994, **6**, 226-228.
2. N. Ahmad and A. G. MacDiarmid, *Synth. Met.*, 1996, **78**, 103-110.
3. J. C. Wu and J. Pawliszyn, *Anal. Chim. Acta*, 2004, **520**, 257-264.
4. A. Bhattacharya, A. De and S. Das, *Polymer*, 1996, **37**, 4375-4382.
5. T. Ohtsuka, T. Wakabayashi and H. Einaga, *J. Electroanal. Chem.*, 1994, **377**, 107-114.
6. F. Li, G.-x. Li, J. Zeng and G.-h. Gao, *J. Appl. Polym. Sci.*, 2014, **131**.
7. M. B. Gonzalez and S. B. Saidman, *Corros. Sci.*, 2011, **53**, 276-282.
8. I. L. Lehr and S. B. Saidman, *Electrochim. Acta*, 2006, **51**, 3249-3255.
9. U. Rammelt, L. M. Duc and W. Plieth, *J. Appl. Electrochem.*, 2005, **35**, 1225-1230.
10. G. Ilangovan and K. C. Pillai, *J. Solid State Electrochem.*, 1999, **3**, 474-477.
11. D. Kowalski, M. Ueda and T. Ohtsuka, *J. Mater. Chem.*, 2010, **20**, 7630-7633.
12. D. Kowalski, M. Ueda and T. Ohtsuka, *Corros. Sci.*, 2007, **49**, 1635-1644.
13. T. Ohtsuka, M. Iida and M. Ueda, *J. Solid State Electrochem.*, 2006, **10**, 714-720.
14. A. Ghicov and P. Schmuki, *Chem. Commun.*, 2009, 2791-2808.
15. F. Beck, R. Kaus and M. Oberst, *Electrochim. Acta*, 1985, **30**, 173-183.

This journal is © The Royal Society of Chemistry [year]

16. M. Pourbaix, *Atlas of Electrochemical Equilibria in Aqueous Solutions*, NACE, Houston, 1974.
17. H. E. Prakasam, O. K. Varghese, M. Paulose, G. K. Mor and C. A. Grimes, *Nanotechnol.*, 2006, **17**, 4285-4291.
18. S. P. Albu, A. Ghicov and P. Schmuki, *Phys. Status Solidi-Rapid Research Letters*, 2009, **3**, 64-66.
19. T. J. LaTempa, X. J. Feng, M. Paulose and C. A. Grimes, *J. Phys. Chem. C*, 2009, **113**, 16293-16298.
20. R. R. Rangaraju, A. Panday, K. S. Raja and M. Misra, *J. Phys. D: Appl. Phys.*, 2009, **42**, 135303.
21. H. Habazaki, Y. Konno, Y. Aoki, P. Skeldon and G. E. Thompson, *J. Phys. Chem. C*, 2010, **114**, 18853-18859.
22. R. R. Rangaraju, K. S. Raja, A. Panday and M. Misra, *Electrochim. Acta*, 2010, **55**, 785-793.
23. S. K. Mohapatra, S. E. John, S. Banerjee and M. Misra, *Chem. Mater.*, 2009, **21**, 3048-3055.
24. Z. H. Zhang, M. F. Hossain and T. Takahashi, *Appl. Cat. B-Env.*, 2010, **95**, 423-429.
25. K. Y. Xie, J. Li, Y. Q. Lai, W. Lu, Z. A. Zhang, Y. X. Liu, L. M. Zhou and H. T. Huang, *Electrochem. Commun.*, 2011, **13**, 657-660.
26. Q. Xu, G. Meng, F. Han, X. Zhao, M. Kong and X. Zhu, *Mater. Lett.*, 2009, **63**, 1431-1434.
27. K. Wagatsuma, K. Hirokawa and N. Yamashita, *Anal. Chim. Acta*, 1996, **324**, 147-154.
28. Y. Konno, E. Tsuji, P. Skeldon, G. E. Thompson and H. Habazaki, *J. Solid State Electrochem.*, 2012, 1-10.
29. G. E. Thompson, *Thin Solid Films*, 1997, **297**, 192-201.
30. H. Habazaki, K. Fushimi, K. Shimizu, P. Skeldon and G. E. Thompson, *Electrochem. Commun.*, 2007, **9**, 1222-1227.
31. S. Yoriya, M. Paulose, O. K. Varghese, G. K. Mor and C. A. Grimes, *J. Phys. Chem. C*, 2007, **111**, 13770-13776.
32. K. Fukami, R. Koda, T. Sakka, Y. Ogata and M. Kinoshita, *J. Chem. Phys.*, 2013, **138**, 094702.

This journal is © The Royal Society of Chemistry [year]